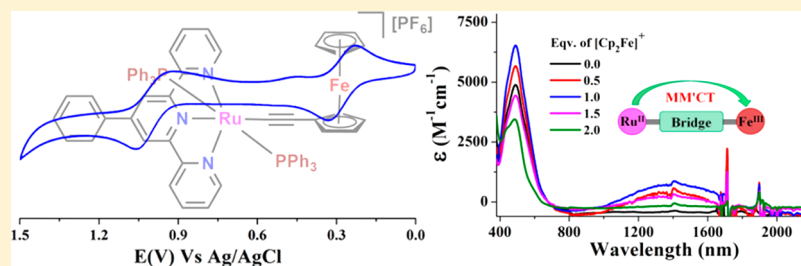


Synthesis, Structure, Electrochemical, and Spectroscopic Properties of Hetero-Bimetallic Ru(II)/Fe(II)-Alkynyl Organometallic Complexes

Amit Sil, Utsav Ghosh, Vipin Kumar Mishra, Sabyashachi Mishra,*[✉] and Sanjib K. Patra*[✉]

Department of Chemistry, Indian Institute of Technology Kharagpur, Kharagpur-721302, West Bengal, India

S Supporting Information



ABSTRACT: A series of heterobimetallic *wire-like* organometallic complexes $[(\text{tpy}-\text{C}_6\text{H}_4-\text{R})(\text{PPh}_3)_2\text{Ru}-\text{C}\equiv\text{C}-\text{Fc}]^+$ ($\text{tpy}-\text{C}_6\text{H}_4-\text{R} = 4'-(\text{aryl})-2,2':6',2''\text{-terpyridyl}$, $\text{Fc} = [(\eta^5\text{-Cp})_2\text{Fe}]$, $\text{R} = -\text{H}, -\text{Me}, -\text{F}, -\text{NMe}_2$ in complexes **5–8**, respectively) featuring ferrocenyl and $4'-(\text{aryl})-2,2':6',2''\text{-terpyridyl}$ ruthenium(II) complexes as redox active metal termini, have been synthesized. Various spectroscopic tools, such as multinuclear NMR, IR spectra, HRMS, CHN analyses, and single crystal X-ray crystallography have been utilized to characterize the heterobimetallic complexes. The electrochemical and UV–vis–NIR spectroscopic studies have been investigated to evaluate the electronic delocalization across the molecular backbones of the Ru(II)–Fe(II) heterobinuclear organometallic *dyads*. Electrochemical studies reveal two well-separated reversible redox waves as a result of successive oxidation of the ferrocenyl and Ru(II) redox centers. The spin density distribution analyses reveal that the initial oxidation process is associated with the Fe(II)/Fe(III) couple followed by one electron oxidation of the ruthenium(II) center. The high K_c value ($0.11\text{--}1.73 \times 10^{12}$) and intense NIR absorption, with molar absorption coefficient (in the order of $10^3 \text{ M}^{-1} \text{ cm}^{-1}$) for the Ru^{II}Fe^{III} mixed-valence species, signify strong electronic communication between the two metal termini. The electronic coupling constant (H_{ab}) has been estimated to be 492 and 444 cm^{-1} for the structurally characterized complexes **6** and **7**, respectively. The redox and NIR absorption features indicate that the mixed-valence system of the heterobinuclear *dyads* belongs to a Robin and Day “class II” system.

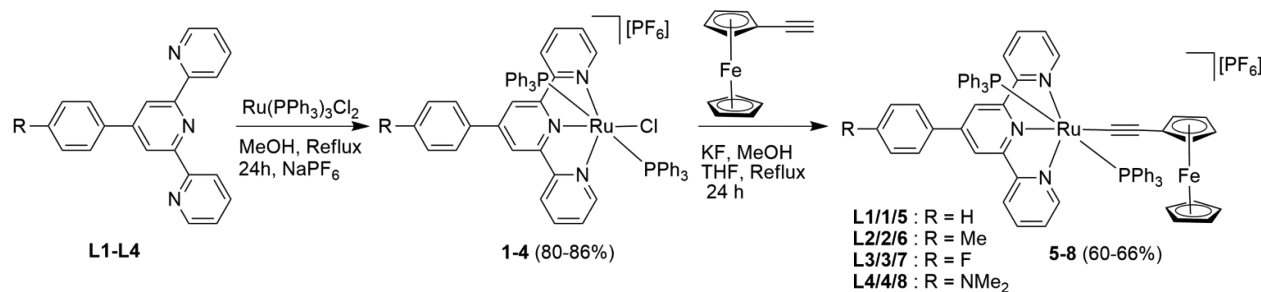
INTRODUCTION

Bimetallic or polymetallic inorganic and organometallic complexes bridged by π -conjugated spacers have received remarkable interest not only for their fascinating mixed valence chemistry¹ but also for their emerging potential applications in molecular electronics,² electrochromism,³ information storage,⁴ ion sensing,⁵ molecular magnetism,⁶ and dye sensitized solar cells.⁷ The pioneering discovery of Creutz–Taube ion,⁸ $[(\text{NH}_3)_5\text{Ru}-\text{pyrazine}-\text{Ru}(\text{NH}_3)_5]^{3+}$, led the scientists to design and develop binuclear complexes to examine the extent of charge delocalization in their mixed-valence states and its fascinating spectroscopic properties.⁹ Homobimetallic complexes capable of imparting remote metal–metal communication across the bridging ligand often generate stable mixed-valence systems and can be coined as molecular *wires*.^{1a,10} More interestingly, special attention has been devoted on the heterobimetallic molecular *wires* having intrinsically redox asymmetry of the metal centers.^{9j,11} Among the heterobimetallic complexes, introduction of ferrocenyl (Fc) acetylide gives a wide diversity of the heterobimetallic complexes which are advantageous for long-range electron transfer.^{9j,11a–n} The synthesis and application of such linear ferrocenyl acetylide

end-capped heterobimetallic complexes, supported by different metal centers, have been developed by various research groups.^{9j,11a–n} Sato and co-workers reported $[(\eta^5\text{-Cp})-(\text{PP})_2\text{Ru}(\text{II})-\text{C}\equiv\text{C}-\text{Fc}]$, while Bruce developed $[\eta^5\text{-Cp}^*(\text{PP})-\text{M}(\text{II})-\text{C}\equiv\text{C}-\text{Fc}]$ ($\text{M} = \text{Ru}, \text{Os}$; $\text{PP} = (\text{PPh}_3)_2, \text{dppe}$ or dppf ; $\text{Cp} = \text{C}_5\text{H}_5, \text{Cp}^* = \text{C}_5\text{Me}_5$) based heterobimetallic complexes to investigate electrochemical communication between Fe(II) and Ru(II)/Os(II) termini.^{11a,g} Long and co-workers have developed a series of heterobimetallic bis(acetylide) ferrocenyl complexes capped with Ru(II)(dppm)₂ [dppm = 1,2-bis-(diphenylphosphino)methane] by varying the electronic nature of the aromatic acetylnyl ligands, and the electrochemical properties have been studied.^{11d} Jia and co-workers reported heterobimetallic ferrocene-ruthenium(II) complexes, $[\text{Fc}(\text{CH}=\text{CH})_3 \text{RuCl}(\text{CO})(\text{PhPy})(\text{PPh}_3)_2]$ showing two partially reversible redox waves for one electron oxidation of the ferrocenyl moiety and the ruthenium(II) metal center, respectively.^{11f} The Zhong group investigated the electrochemical and consequent NIR absorbing properties of a series

Received: August 29, 2018

Scheme 1. Synthesis of the Hetero-bimetallic Complexes (5–8)



of bis-tridentate complexes $[\text{Ru}(\text{Fc}(\text{d}p\text{b}))(\text{tpyR})]^+(\text{Fc}(\text{d}p\text{b}) = 2\text{-deprotonated form of } 1,3\text{-di}(2\text{-pyridyl})\text{-5-ferrocenylbenzene; tpyR} = 2,2':6',2''\text{-terpyridyl derivative})$, consisting of ferrocene and cyclometalated ruthenium centers by varying the auxiliary ligands.^{11s} Later, Zhong and co-workers studied cyclometalated and noncyclometalated ruthenium-ferrocenyl complexes and demonstrated relatively weaker intermetallic interaction in the case of noncyclometalated heterobimetallic complexes.^{11m} Later, Chen and co-workers developed a ruthenium(II) complex of 1,3-bis(2-pyridylimino)isoindolate capped with an acetynyl ferrocenyl unit, showing a remarkable K_c (comproportionation constant) value of 4.18×10^{10} .^{9j} Recently, the Chen group examined ruthenium(II) complexes of 2,3,5,6-tetrakis(2-pyridyl)pyrazine capped with ferrocenyl acetylide exhibiting remarkable NIR absorption at 1230 nm with high K_c value of 2.82×10^8 revealing efficient electronic communication between ruthenium(II) and the ferrocenyl moiety.¹¹ⁿ These complexes exhibited promising metal–metal communication depending on the electronic and redox nature of organometallic congeners. In ferrocenyl acetylide capped heterobimetallic complexes, the metal-to-metal charge transfer (MMCT) from one metal site to the other metal center depends on the electrochemical nature of the redox active metal termini $[\text{M}]$ as well as the nature of the π -conjugated bridging spacers and ligands. When the one-electron reduction potential of the ferrocenyl unit (Fc) is lower than that of the $[\text{M}]$ moiety, the electrochemical communication is operative from $[\text{M}]$ to Fc and *vice versa*. 2,2':6',2''-Terpyridine (*tpy*) and their structural analogs exhibit versatile coordination chemistry with most of the transition metal cations. It is well documented in the literature that the ligands with different electronic nature influence the redox potential of the metal centers and splitting of redox wave arising from electronic interaction.^{11c,q} The metal–metal communication in mixed-valence systems depends on various factors such as the electronic nature of the ligand, the length of the bridging spacer between the two redox active metal termini, and the intrinsic properties of the terminal metal centers. Typically, the mixed-valence systems are categorized into three classes (class I to class III) depending upon the degree of metal–metal electronic communication according to Robin and Day classification¹² and Hush theoretical analysis.¹³ Electrochemistry and spectroscopic measurement in the near-infrared region (NIR) have been utilized to estimate the magnitude of electronic communication between the two redox active metal centers. As a result, the judicious selection of ligands with proper electronic nature is important for tuning the electronic communication along molecular backbones.

In this work, a series of acetylide bridged heterobimetallic Ru(II)/Fe(II) *dyads*, $[(\text{tpy}-\text{C}_6\text{H}_4\text{-R})(\text{PPh}_3)_2\text{Ru}-\text{C}\equiv\text{C}-\text{Fc}]^+$

($\text{R} = \text{-H, -Me, -F, -NMe}_2$; $\text{Fc} = [(\eta^5\text{-Cp})_2\text{Fe}]$), have been synthesized by varying the electronic nature of the ligands. The heterobimetallic complexes have been characterized by different spectroscopic tools including multinuclear NMR, HRMS, and single crystal X-ray diffraction studies. The electrochemical and UV–vis–NIR spectroscopic studies have been performed to evaluate the electronic delocalization across the molecular backbones of the heterobimetallic complexes. Moreover, spin density distribution analysis and TD-DFT studies have also been carried out to understand the electronic communication between the two redox termini in this series of Ru(II)/Fe(II) organometallic *dyads*.

RESULTS AND DISCUSSION

Synthesis and Characterization. A series of 4'-(aryl)-2,2'-6',2''-terpyridyl ligands (aryl = phenyl, tolyl, 4-fluorophenyl, 4-(dimethylamino)phenyl for **L1–L4**, respectively) have been synthesized by varying the electron donating or withdrawing nature of the 4'-aryl group to investigate the role of terminal group on electronic communication in the targeted heterobimetallic complexes. Condensation of aryl aldehyde with 2 equiv of acetylpyridine in the presence of ammonia as a base led to the formation of the desired terpyridyl ligands.¹⁴ Formation of the ligands was ascertained by ¹H, ¹³C NMR and mass spectrometry (SI). The corresponding Ru(II) complexes (**1–4**), $[(\text{tpy}-\text{C}_6\text{H}_4\text{-R})(\text{PPh}_3)_2\text{RuCl}][\text{PF}_6]$ ($\text{R} = \text{-H, -Me, -F, -NMe}_2$) were synthesized by the reaction of 4'-(aryl)-2,2'-6',2''-terpyridine (**L1–L4**) and $[\text{Ru}(\text{PPh}_3)_3\text{Cl}_2]$ in degassed refluxing methanol. After filtration of the reddish brown reaction mixture through a pad of Celite, the filtrate was dried under reduced pressure. The solid residue was subsequently dissolved in a minimum amount of distilled MeOH, and the solution was finally treated with 2 equiv of NaPF₆. The analytically pure products (**1–4**) were obtained with a high yield of 80–86% after subsequently being washed with a copious amount of Et₂O, followed by recrystallization by layering diethyl ether on an acetonitrile solution of the complexes. In ¹H NMR studies of Ru(II) complexes (**1–4**), the protons attached to the carbon next to the nitrogen atom of the pyridyl ring resonate at 9.03–9.05 ppm, which is substantially downfield shifted by 0.35 ppm with respect to the free 4'-(aryl)-2,2'-6',2''-terpyridines, revealing coordination of the terpyridyl moiety to the metal center. In ¹H NMR, the characteristic singlet peak for the methyl protons of complexes **2** and **4** resonates at 2.49 ppm (CH₃) and 3.10 ppm (NMe₂), respectively. The signals for the other aromatic protons are observed in the region of 7.08–8.45 ppm whereas the aromatic carbons resonated in the region of 120.1–158.3 ppm. A sharp singlet at 20.1–20.4 ppm in ³¹P{¹H} NMR of **1–4** confirms the presence of two coordinated PPh₃ ligands having similar

Table 1. Important Bond Distances and Angles for Complexes 3, 6, and 7

Complex 3		Complex 6		Complex 7	
Bond Distances (Å)					
Ru1–Cl1	2.4469(7)	Ru1–P1	2.380(2)	Ru1–P1	2.3848(12)
Ru1–P1	2.4131(7)	Ru1–P2	2.385(2)	Ru1–P2	2.3786(12)
Ru1–P2	2.4245(7)	Ru1–N3	2.104(7)	Ru1–N3	2.092(4)
Ru1–N3	2.117(2)	Ru1–N2	2.021(6)	Ru1–N2	2.009(3)
Ru1–N1	2.098(2)	Ru1–N1	2.120(6)	Ru1–N1	2.097(4)
Ru1–N2	1.964(2)	Ru1–C23	2.057(9)	Ru1–C22	2.052(5)
		C23–C24	1.149(11)	C22–C23	1.187(7)
Bond Angles (deg)					
P1–Ru1–Cl1	88.93(2)	P1–Ru1–P2	174.63(9)	P2–Ru1–P1	173.51(5)
P1–Ru1–P2	174.50(2)	N3–Ru1–P1	90.14(19)	N3–Ru1–P1	92.99(10)
P2–Ru1–Cl1	85.57(2)	N3–Ru1–P2	90.07(19)	N3–Ru1–P2	88.39(10)
N3–Ru1–Cl1	104.25(6)	N2–Ru1–P1	93.82(19)	N2–Ru1–P1	94.34(10)
N3–Ru1–P1	89.69(6)	N2–Ru1–P2	91.48(18)	N2–Ru1–P2	92.16(10)
N3–Ru1–P2	91.84(6)	N2–Ru1–N3	78.0(3)	N2–Ru1–N3	77.85(13)
N1–Ru1–Cl1	98.00(6)	N2–Ru1–N1	77.5(3)	N2–Ru1–N1	78.30(14)
N1–Ru1–P1	90.48(6)	N2–Ru1–C23	177.9(3)	N2–Ru1–C22	177.84(16)
N1–Ru1–P2	90.10(6)	N1–Ru1–P1	89.94(18)	N1–Ru1–P1	90.37(10)
N2–Ru1–Cl1	176.78(6)	N1–Ru1–P2	92.09(18)	N1–Ru1–P2	90.92(10)
N2–Ru1–P1	91.75(6)	N3–Ru1–N1	155.5(3)	N1–Ru1–N3	156.10(15)
N2–Ru1–P2	93.73(6)	C23–C24–C25	175.4(10)	C22–C23–C24	177.1(6)
		Ru1–C23–C24	178.5(8)	Ru1–C22–C23	177.5(4)
Torsional Angles (deg)					
C9–C8–C16–C21	34.69	C7–C8–C16–C17	–34.78	C7–C8–C16–C17	–36.06
C7–C8–C16–C17	36.02	C9–C8–C16–C21	–33.17	C9–C8–C16–C21	–35.80

coordination environment. In FTIR spectra, the stretching frequency at 840–845 cm^{-1} validates the presence of PF_6^- as a counteranion. Finally, HRMS spectrometry of the Ru(II) complexes (1–4) confirms their formation by revealing the molecular ion peaks ($[\text{M}-\text{PF}_6]^+$) at m/z of 970.1848, 984.1983, 988.1804, and 1013.2243, respectively (SI). The isotopic distribution patterns for the molecular ion peaks obtained from the experimental data are in perfect agreement with the simulated data for all the Ru(II) complexes. After successful synthesis of the Ru(II) complexes (1–4), incorporation of ferrocenyl alkynyl moiety was accomplished to furnish the desired heterobimetallic complexes (5–8). The heterobimetallic wires $[(\text{tpy}-\text{C}_6\text{H}_4-\text{R})(\text{PPh}_3)_2\text{Ru}-\text{C}\equiv\text{C}-\text{Fc}]^+$ ($\text{R} = \text{H}, \text{Me}, \text{F}, \text{NMe}_2$; $\text{Fc} = [(\eta^5\text{-Cp})_2\text{Fe}]$) (5–8) were synthesized by treating the chloride coordinated Ru(II) complexes (1–4) with the ethynyl ferrocene in refluxing MeOH/THF solution in the presence of KF (Scheme 1). The reaction was accomplished with a distinct color change of the reaction mixture from brownish to intense wine red. The solvent was evaporated after completion of the reaction, and the product was washed with diethyl ether and hexanes to remove the unreacted ethynyl ferrocene. The synthesized complexes were purified by neutral alumina column chromatography using methanol as an eluent. The second band was collected as analytically pure heterobimetallic complexes (5–8) with a moderate yield (60–66%). The complexes were characterized unambiguously by multinuclear NMR, FTIR, and HRMS spectrometry as well as by elemental analyses. In ^1H NMR spectra of the heterobimetallic complexes (5–8), the protons adjacent to the pyridyl-N resonate at 8.80–8.87 ppm with an upfield shift of about 0.22 ppm relative to that of the complexes 1–4. The remaining aromatic protons resonate in the region of 6.88–7.94 ppm whereas the ferrocenyl protons resonate in the region at 4.13–4.46 ppm as multiplets. The

characteristic singlet for the methyl protons of complexes 6 and 8 resonates at 2.16 (CH_3) and 3.11 ppm (NMe_2), respectively. In $^{13}\text{C}\{^1\text{H}\}$ NMR spectra of the heterobimetallic complexes (5–8), the aromatic carbons exhibit signals in the region of 120.1–157.8 ppm whereas the ferrocenyl carbons appear in the region of 64.6–70.1 ppm, revealing the incorporation of ferrocenyl moiety. The methyl carbon for complexes 6 and 8 resonate at 21.6 (CH_3) and 40.5 ppm (NMe_2), respectively. In $^{31}\text{P}\{^1\text{H}\}$ NMR spectra, the singlet resonances at 27.9–28.5 ppm are attributed to the coordinated PPh_3 , having a downfield shift of 7 ppm compared to the coordinated PPh_3 in the mononuclear Ru(II) complexes (1–4). Moreover, the presence of counteranion is confirmed by $^{31}\text{P}\{^1\text{H}\}$ NMR showing multiplet at about –143.6 ppm as well as by IR spectra exhibiting $\bar{\nu}(\text{PF}_6)$ at 840–844 cm^{-1} . Furthermore, the characteristic $\bar{\nu}(\text{Ru}-\text{C}\equiv\text{C})$ stretching frequency for all the heterobimetallic *dyads* (5–8) appears at 2063–2070 cm^{-1} . This further confirms the formation of Ru(II)-acetylide σ -bond by replacement of the coordinated chloride ligand. Finally, HRMS analyses of the heterobimetallic *wire*-like complexes (5–8) reveal the molecular ion peaks ($[\text{M}-\text{PF}_6]^+$) at 1144.2102, 1158.2356, 1162.2069, and 1187.2685, respectively, with perfect agreement in the isotropic distribution pattern to the simulated pattern.

Solid State Structure. The molecular structures of the synthesized complexes have been determined by X-ray crystallography to gain an insight into the structure property relationship. The reddish brown colored single crystals for the complexes 3 and 6 suitable for single crystal X-ray diffraction were grown by layering hexanes on DCM solution, whereas complex 7 was crystallized upon layering hexanes on CHCl_3 solution in a sealed glass tube. In mononuclear Ru(II) complex 3, the P1–Ru1–N1, P1–Ru1–N2, and P1–Ru1–N3 bond angles are in the range of 89.69(6)°–91.75(6)° whereas the

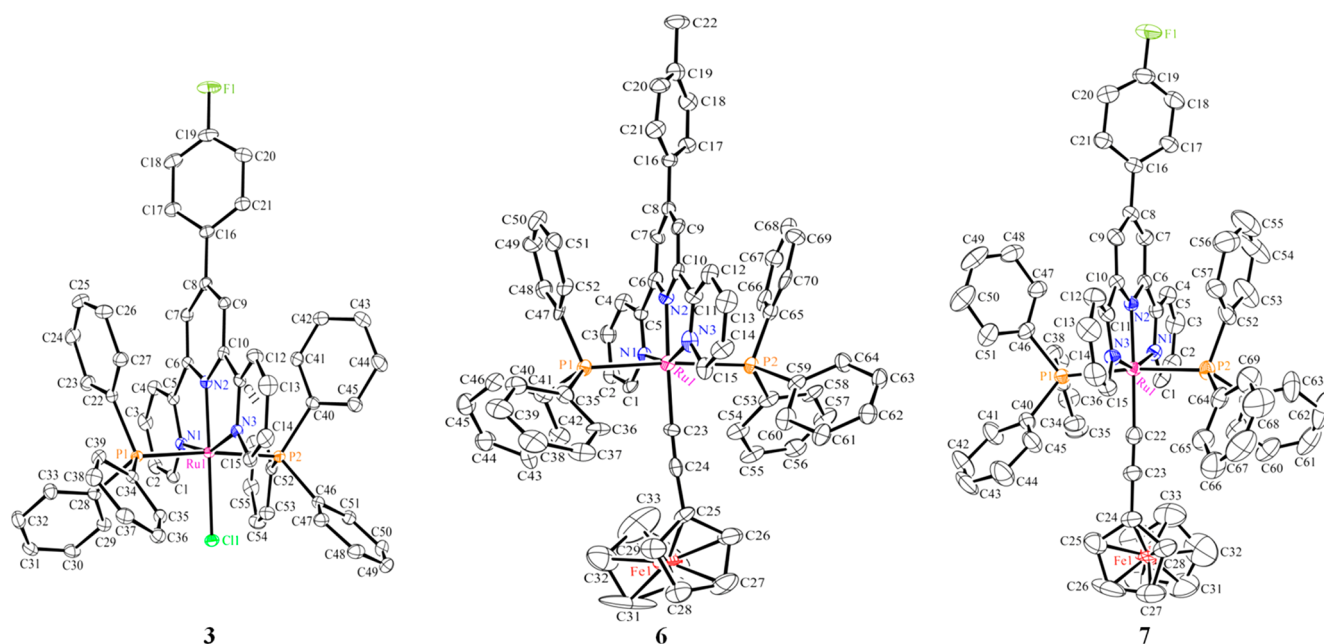


Figure 1. ORTEP²⁵ diagrams of complexes **3**, **6**, and **7**. Hydrogen atoms are omitted for the sake of clarity. The thermal ellipsoids are drawn at 40% probability.

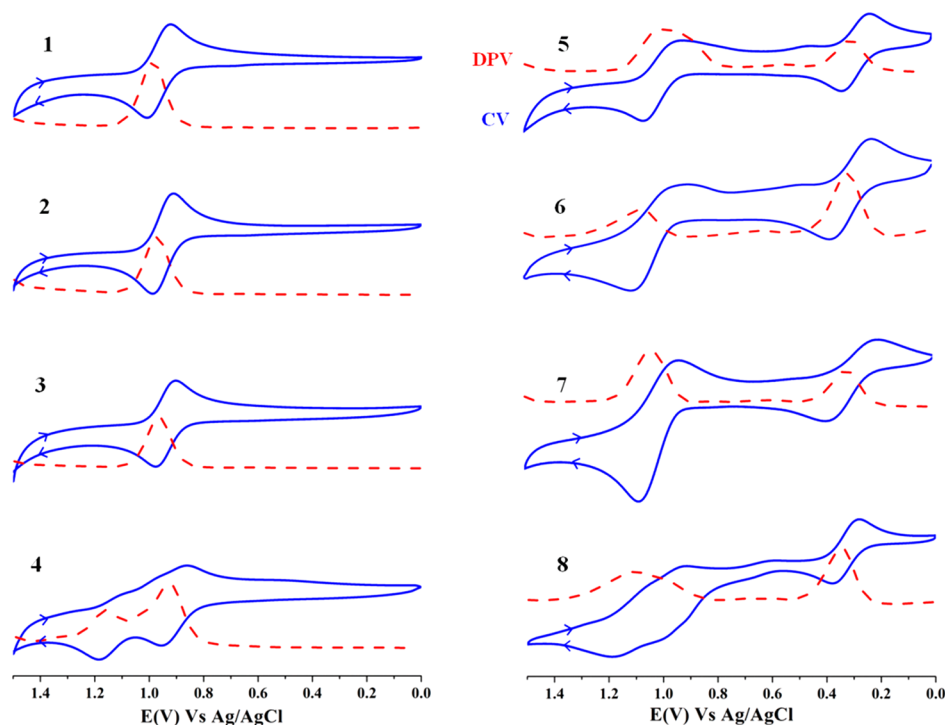


Figure 2. Cyclic voltammograms (CV) and differential pulse voltammograms (DPV) of the Ru(II) complexes (**1–4**) and heterobinuclear ruthenium(II)-ferrocenyl organometallic *dyads* (**5–8**) in DCM at a scan rate of 100 mV s^{-1} . Potentials are given relative to the Ag/AgCl reference electrode.

bond angles for P2–Ru1–N1, P2–Ru1–N2, and P2–Ru1–N3 are found as $90.10(6)^\circ$ – $93.73(6)^\circ$, respectively, attributing that the two PPh₃ ligands adopt nearly orthogonal arrangement above the planar NNN terpyridyl ring. The P1–Ru1–Cl1 and P2–Ru1–Cl1 bond angles are $88.93(2)^\circ$ and $85.57(2)^\circ$, respectively, ascribing that Cl1 is positioned orthogonally to both the P atoms (P1 and P2) of the two PPh₃ ligands. The P1–Ru1–P2 bond angle is $174.50(2)^\circ$ for complex **3**, suggesting the *trans* orientation of the two PPh₃ ligands.

Thus, the molecular structure of complex **3** reveals a hexacoordinated Ru(II) center forming a slightly distorted octahedron formed by three “N” donors of the terpyridyl unit, one chloride, and two *trans*-positioned “P” donors of PPh₃. In complex **6**, the C23–C24–C25 and Ru1–C23–C24 angles are $175.4(10)^\circ$ and $178.5(8)^\circ$, respectively, revealing the almost linear linkage of –Fc–C≡C– and –Ru–C≡C–. Similarly, the linear linkages of –Fc–C≡C– and –Ru–C≡C– are manifested for complex **7** showing the C22–C23–C24

Table 2. Electrochemical Data for Ru(II) Complexes (1–4) and Hetero-binuclear Ruthenium(II)-ferrocenyl Organometallic Wires (5–8)

Complex	$E_{1/2}(1),^a$ V	$E_{1/2}(2),^a$ V	$E_{1/2}(3),^a$ V	$\Delta E_{1/2},^b$ mV	K_c^c
1		0.930(96)			
2		0.948(94)			
3		0.962(95)			
4		0.900(91)	1.14(115)		
5	0.283(104)	0.995(114)		712	1.08×10^{12}
6	0.296(140)	1.02(165)		724	1.73×10^{12}
7	0.299(137)	1.01(180)		711	1.04×10^{12}
8	0.326(94)	0.980(78)	1.11(115)	654	1.12×10^{11}

^aCorresponding $E_{pa} - E_{pc}$ values (in mV) in parentheses. ^b $\Delta E_{1/2} = E_{1/2}(2) - E_{1/2}(1)$. ^c $K_c = \exp(\Delta E_{1/2}/25.69)$ at 298 K.

and Ru1–C22–C23 angles are of 177.1(6)° and 177.5(4)°, respectively. The P1–Ru1–N1, P1–Ru1–N2, and P1–Ru1–N3 bond angles for complex 6 are in the range of 89.94(18)°–93.82(19)° whereas the bond angles for P2–Ru1–N1, P2–Ru1–N2, and P2–Ru1–N3 are found in the range of 90.07(19)°–92.09(18)°, respectively, ascribing the nearly orthogonal position of two PPh₃ ligands above the planar NNN terpyridyl moiety. Similar bond angles (Table 1) are also observed for complex 7 manifesting the identical coordination environment of the PPh₃ ligands. Thus, in the heterobimetallic complexes (6 and 7) the Ru(II) center is also hexacoordinated showing slightly distorted octahedral geometry in which two axially bonded “P” donors of PPh₃ are *trans* oriented. The equatorial plane of the Ru(II) centers is surrounded by the three “N” atoms of the terpyridyl unit and one “C” atom of acetylide. The Ru...Fe distances for complexes 6 and 7 are found to be 6.192 and 6.221 Å, respectively. The two cyclopentadienyl rings in the ferrocenyl group are approximately eclipsed as manifested by the rotational angles which are in the range of 9.31–12.14 Å and 2.26–6.66 Å for the complexes 6 and 7, respectively. The ORTEP diagrams of the complexes 3, 6, and 7 are depicted in Figure 1, while the selected bond angles and bond lengths are listed in Table 1.

Electrochemical Studies. The electrochemical properties of the mononuclear Ru(II) (1–4) and heterobimetallic Ru(II)/Fe(II) (5–8) complexes were investigated using cyclic voltammetry (CV) and differential pulse voltammetry (DPV) at a scan rate of 100 mVs⁻¹ using ⁿBu₄NPF₆ (0.1 M) as supporting electrolyte, Ag/AgCl reference electrode, and Pt disc working electrode in dry dichloromethane. The Ru(II) complexes (1–4) exhibit a reversible redox wave at 0.93 V, 0.948 V, 0.962 V, and 0.90 V, respectively, due to the oxidation (Ru^{II}/Ru^{III}) process. The potential difference ($E_{pa} - E_{pc}$) of the individual Ru^{II}/Ru^{III} redox couple for all the complexes were around 91–96 mV ascribing good correlation with one electron Nernstian process. Unlike others, complex 4 showed a quasi-reversible oxidation wave at higher positive potential ($E_{pa} = +1.14$ V), which is likely to be associated with the oxidation of the -NMe₂ group resulting *in situ* generation of radical cation, Me₂N^{•+}. Interestingly, for all the heterobinuclear ruthenium(II)-ferrocenyl organometallic dyads (5–8), two distinctly separated reversible redox waves were observed due to the presence of the redox active ferrocenyl (Fc) and ruthenium(II) centers (Figure 2, Table 2). For all the heterobimetallic complexes, the reduction potential of the Fc/Fc⁺ couple and Ru^{II}/Ru^{III} couple showed substantial cathodic and anodic shift, respectively, with respect to reduction potential of ethynylferrocene ($E_{1/2} = 0.76$ V) and the Ru(II) complexes (1–4) (Figure 2 and SI). For example,

the two successive reversible redox waves occurred at 0.283 V (Fc/Fc⁺) and 0.995 V (Ru^{II}/Ru^{III}), respectively, with a potential difference [$\Delta E_{1/2} = E_{1/2}(2) - E_{1/2}(1)$] of 712 mV between the two consecutive redox waves in complex 5. The formation of Ru–C≡C–Fc σ -bond by the replacement of chloride ligand in Ru(II) complexes (1–4) increases the reduction potential of the Ru(II) center (in complexes 5–8) because of appreciable Ru...Fe metal–metal electronic interaction.¹¹ⁿ However, the reduction potential for the ferrocene/ferrocenium (Fc/Fc⁺) couple occurred in less positive potential in comparison to ethynyl ferrocene due to combined inductive and electron delocalization effect induced by the Ru(II) center. The assignment of the redox potentials was supported by the electrochemical studies as described in the literature with analogous heterobimetallic wires combined with ruthenium(II) and ferrocenyl redox centers.^{11a–n} The separation between the two successive oxidation waves ($\Delta E_{1/2}$) and the comproportionation constant [$K_c = \exp(-\Delta E_{1/2}/25.69)$ at 298 K] are the critical parameters to assess thermodynamic stability of the mono-oxidized states (Ru^{II}/Fe^{III}) and the electronic delocalization between the two redox termini through the molecular backbones. The corresponding K_c of complex 5 has been estimated to be 1.08×10^{12} ascribing the good stability of the Ru^{II}/Fe^{III} mixed-valence intermediate as a result of the inherent redox asymmetric nature of the metal centers. Similarly, the heterobimetallic complexes 6 and 7 also exhibited two successive reversible redox waves showing $E_{1/2}$ at 0.296 and 0.299 V, respectively, originating from oxidation of the Fe(II)/Fe(III) (Fc/Fc⁺) couple, while the consecutive $E_{1/2}$ owing to the oxidation of the Ru(II)/Ru(III) couple occurred at 1.02 and 1.01 V, respectively. The comproportionation constants for the complexes 6 and 7 were estimated to be 1.73×10^{12} and 1.04×10^{12} respectively. In contrast, complex 8 showed two successive redox processes occurred at 0.326 and 0.98 V, respectively, with K_c of 1.12×10^{11} , along with a third redox process at relatively higher positive potential ($E_{1/2} = 1.11$ V) attributed to the oxidation of the -NMe₂ group (N⁰/N^{•+}). However, the degree of metal–metal interaction cannot be evaluated directly from the wave separation of the sequential oxidation of ferrocenyl and ruthenium center ($\Delta E_{1/2}$) due to the structural asymmetry and inherent differences in redox potentials of these systems.^{9d,11n} It should also be noted that the K_c is determined not only by the resonance contribution (ΔG_r) but also by the several nonresonance contribution (ΔG_{nr}) by a significant extent.¹⁵ The careful examination of the electrochemical data (Table 2) suggests that the redox potentials are dependent on the electronic nature of the functional terpyridyl moieties, but to a lesser degree.

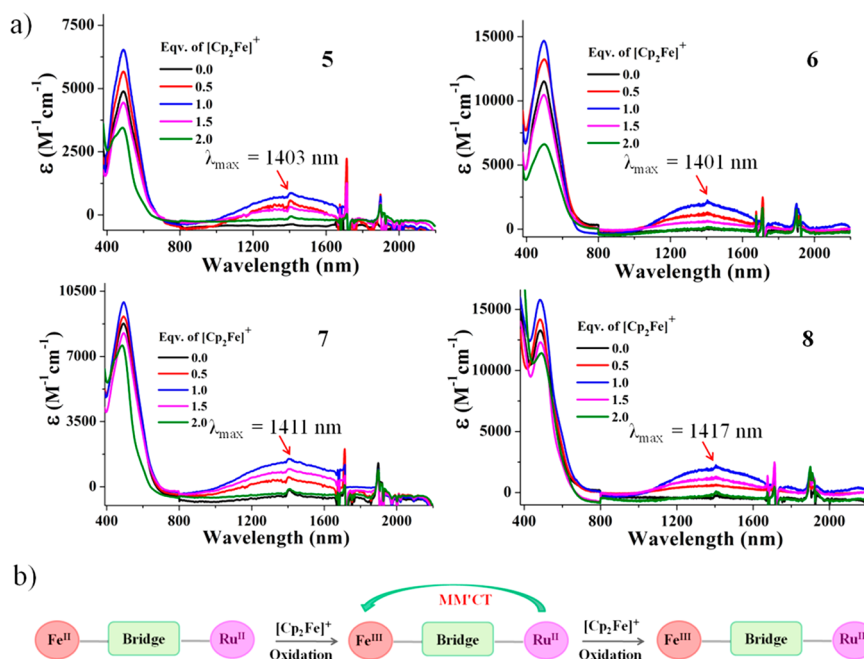


Figure 3. a) UV-vis-NIR spectra of binuclear Ru(II) complexes (5–8) in DCM after the gradual addition of organometallic oxidant $[(\eta^5\text{-Cp})_2\text{Fe}][\text{BF}_4]$. b) Illustration of MM'CT transition inducing NIR absorption in the heterobinuclear Ru(II)/Fe(II) complexes.

UV-vis-NIR Studies. For all the Ru(II) complexes (1–4), the intense absorption bands in the UV region appeared in the range of 270–325 nm which is presumably due to the $\pi\text{-}\pi^*$ transition associated with the terpyridyl moiety (Figure S26, SI). The Ru(II) complexes (1–4) exhibited broad absorption bands in the visible region of λ_{max} at 492–507 nm ($\epsilon = 0.67\text{--}1.23 \times 10^4 \text{ M}^{-1} \text{ cm}^{-1}$) due to metal-to-ligand charge transfer (MLCT) transitions.¹⁶ On the other hand, the heterobimetallic complexes (5–8) exhibited strong absorption bands in the region of 312–316 nm ($\epsilon = 3.68\text{--}4.44 \times 10^4 \text{ M}^{-1} \text{ cm}^{-1}$) due to the ligand centered $\pi\text{-}\pi^*$ transition. The absorption band in the visible region centered at 492–499 nm ($\epsilon = 0.51\text{--}1.37 \times 10^4 \text{ M}^{-1} \text{ cm}^{-1}$) in the complexes 5–8 was ascribed to metal-to-ligand charge transfer transitions (MLCT for both the Ru(II) and Fe(II) centers). High K_c values due to the inherent redox asymmetry prompted us to explore the UV-vis-NIR absorbing property of the heterobimetallic wires. To investigate the electron transfer process of complexes 5–8, the changes in their UV-vis-NIR spectra were investigated upon incremental charging of $[(\eta^5\text{-Cp})_2\text{Fe}][\text{BF}_4]$ in DCM at 25 °C. Interestingly, upon treating with incremental equivalent (0–1.0) of organometallic oxidant $[(\eta^5\text{-Cp})_2\text{Fe}][\text{BF}_4]$, the MLCT band ($\lambda_{\text{max}} = 492\text{--}498 \text{ nm}$) gradually increased for all the heterobimetallic complexes. More importantly, a new broad band started to appear in the NIR region centered at 1401–1417 nm with remarkable ϵ value in the range of $1.11\text{--}1.65 \times 10^3 \text{ M}^{-1} \text{ cm}^{-1}$ as a result of MM'CT (metal-to-metal charge transfer) from Ru^{II} to Fe^{III} metal center. On addition of 1 equiv of oxidant, the ferrocenyl groups were completely oxidized (Fe^{II} to Fe^{III}) inducing the MM'CT transition with the maximum ϵ value. Adding more than 1 equiv of oxidant, the intensity of the MLCT band ($\lambda_{\text{max}} = 492\text{--}498 \text{ nm}$) started to diminish with concomitant disappearance of the MM'CT band in the NIR region, illustrating decrease in electronic communication between the heterobimetallic redox centers because of gradual conversion of Ru^{II}Fe^{III} mixed-valence species to Ru^{III}Fe^{III} (Figure 3). The large $\Delta E_{1/2}$ (654–724

mV) and K_c ($0.11\text{--}1.73 \times 10^{12}$) values of the heterobimetallic complexes (5–8) are the characteristic of a “class III” mixed-valence system.¹² However, for the heterobimetallic complexes, the large $\Delta E_{1/2}$ and K_c values are presumably caused by both the redox dissymmetry and inherent differences in redox potentials.^{11d,n} To gain more insight into the extent of electronic communication, the electronic coupling constants have been calculated following Hush’s theory. For the heterobimetallic wires (5–8), the observed half-width, $\Delta\nu_{1/2}$ ($1930\text{--}2823 \text{ cm}^{-1}$) was found to be comparable to the calculated half-width values ($1745\text{--}2029 \text{ cm}^{-1}$) as established by the equation $\Delta\nu_{1/2} = [2310(\nu_{\text{max}} - \Delta G^0)]^{1/2}$ (where ΔG^0 is estimated from $\Delta E_{1/2}$ as upper bound value) according to Hush theory assuming two-state model for electron transfer in unsymmetrical bimetallic complexes.^{9p,13} This suggests that the heterobimetallic dyads (5–8) belong to the “class II” mixed-valence complexes.¹² In view of these redox and absorption features, it can be concluded that the mixed-valence intermediates of the heterobimetallic dyads likely belong to the “class II” mixed-valence system.^{11d,n,12} The electronic coupling matrix element (H_{ab}), which determines the extent of charge delocalization in mixed-valence compounds, has been evaluated from the NIR absorption band induced by the MM'CT transition. We are able to calculate the electronic coupling constant for complexes 6 and 7 which have been structurally characterized by single crystal X-ray crystallography giving intermetallic distances (R) of 6.19 and 6.22 Å, respectively. The electronic coupling constants of the mixed-valence complexes 6 and 7 were calculated by the equation $H_{\text{ab}} = [\{(2.05 \times 10^{-2})(\nu_{\text{max}}\epsilon_{\text{max}}\Delta\nu_{1/2})^{1/2}\}/R]$ considering “class II” mixed-valence complexes where ϵ_{max} , ν_{max} , and $\Delta\nu_{1/2}$ are molar extinction coefficient, absorption maximum, and observed bandwidth at half-maximum height (in wave numbers) of NIR absorption band, respectively. The electronic coupling constant (H_{ab}) of 6 is estimated to be 492 cm^{-1} . Similarly, complex 7 exhibits observed half-width as 2119 cm^{-1} ,

calculated half-width as 1784 cm^{-1} , and electronic coupling constant, $H_{ab} = 444\text{ cm}^{-1}$ (Table 3).

Table 3. Electrochemical Data of Hetero-binuclear Ruthenium(II)-Ferrocenyl Organometallic Wires (5–8)

Complex	λ_{\max} (nm)	ϵ_{\max} ($\text{M}^{-1}\text{cm}^{-1}$)	ν_{\max} (cm^{-1})	$\Delta\nu_{1/2}^{\text{obsd}}$ (cm^{-1}) ^a	$\Delta\nu_{1/2}^{\text{calcd}}$ (cm^{-1}) ^b	H_{ab} (cm^{-1}) ^c
5	1403	1114	7137	1930	1795	
6	1401	1223	7158	2823	1745	492
7	1411	1315	7112	2119	1784	444
8	1417	1650	7057	2336	2029	

^aObserved half-width of MM'CT band. ^bCalculated half-width following the equation $\Delta\nu_{1/2} = [2310(\Delta\nu_{\max} - \Delta G^0)]^{1/2}$ where ΔG^0 is estimated from $\Delta E_{1/2}$ as the upper bound value.¹³ ^cElectronic coupling constant for class II mixed-valence compounds.

Theoretical Studies. To gain insight into the electronic structures and spectroelectrochemical properties further, density functional theoretical studies have been performed for all the heterobinuclear wires. The optimized geometries of the complexes are found to be in good agreement with the corresponding molecular structures obtained from SCXRD studies, such as for compounds 6 and 7 (Table S4). The frontier molecular orbitals of the complexes in their neutral and cationic forms were analyzed by doing a molecular orbital decomposition analysis over different “fragments” of the complexes. The contributions of the two metal centers, the acetylide group, and the Cp groups to the frontier MOs are summarized in Tables S6 and S7. The HOMO of neutral complex 5 is primarily contributed by “Fc–C≡C” (64%) and a relatively smaller contribution from the ruthenium(II) center (23.8%). In contrast, the lowest occupied molecular orbital (LUMO) of the complex (5) has predominant contribution from the 4'-(aryl)-2,2':6,2''-terpyridyl moiety (87.6%) with a minor contribution from the Ru(II) metal center (3.85%). The contributions of the different fragments in the HOMO/LUMOs for the other complexes (6–8) are similar to that of 5 as depicted in Figure 4. Moreover, the spin density calculation of the corresponding singly oxidized species of complexes 5

and 6 (i.e., 5⁺ and 6⁺) have been performed to predict the origin of the first one-electron reversible oxidation process. Interestingly, the electron spin density distribution in the mono-oxidized species is predominately delocalized over the ferrocenyl moiety (>90%), whereas very slight spin density distribution is resident on the Ru(II) center (Figure 5). The

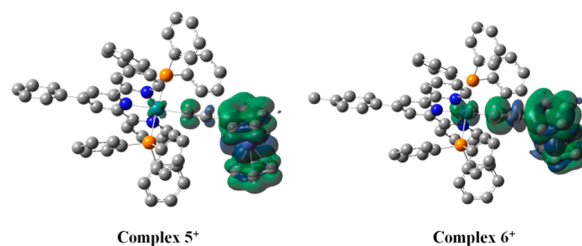


Figure 5. Spin density distributions in mono-oxidized complexes, 5⁺ and 6⁺. Contour values: $\pm 0.0004\text{ e/bohr}^3$.

higher spin density on the ferrocenyl moiety than that on the Ru(II) center clearly indicates that the first one-electron oxidation processes (0.28–0.32 V) in the studied bimetallic complexes are associated with the Fc/Fc⁺ couple, while the oxidation states of the Ru(II) centers remain unperturbed. Moreover, upon one-electron oxidation, the geometries of these complexes are found to undergo minimal changes. The most important changes in the geometry of the oxidized species occur in the form of (a) shortening of Ru(II)–C_{acetylide}; (b) elongation of the “C≡C” bond (acetylide); and (c) increasing in the Fe–Cp distances (Table S5). The changes in the bond lengths indicate that the one-electron oxidation in the complexes is accompanied by a net charge transfer from the Ru(II) metal center to the Fe(III) center via the alkyne bridge. This is further confirmed by the decrease in the C≡C stretching frequency estimated in the oxidized species (from 2245 cm^{-1} in 5 to 2173 cm^{-1} in 5⁺). To obtain more detailed insight into the electronic transition and spectroscopic properties in the series of synthesized heterobimetallic dyads, the time-dependent density functional theory (TDDFT) was performed for complex 5 and its corresponding singly oxidized

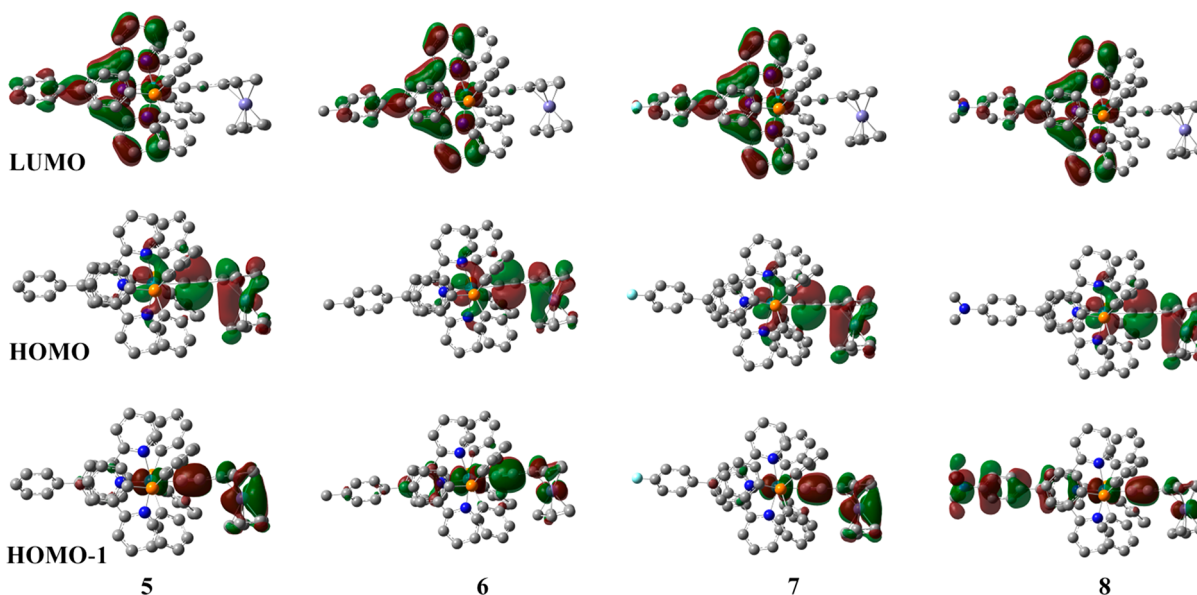


Figure 4. Selected frontier molecular orbitals of the heterobinuclear complexes. Contour values: $\pm 0.02\text{ (e/bohr}^3)^{1/2}$.

species (5^+) as a case study. The UV–vis–NIR spectra obtained from TDFT calculations of complex **5** and its oxidized form are shown in Figure S31. The computed UV–vis absorption spectrum appears in the region of 450 to 550 nm and is in good agreement with experimental absorption. Additionally, the computed absorption spectrum of the singly oxidized species, 5^+ shows an absorption band in the NIR region (centered at 1127 nm), albeit with very low oscillator strength. This band was absent in the neutral complexes. The NIR band at λ_{max} of 1127 nm mainly arises from the electronic transition from the highest occupied spin–orbital (HOSO)-26 to the lowest unoccupied spin orbital LUSO (53%), with additional minor contribution from HOSO-25 and HOSO-24 to LUSO transitions (18% and 9%, respectively) (Figure S32). The HOSO-26 spin orbital is found to be dominated by the electronic population on the ruthenium(II) center along with the 4'-phenyl-2,2':6',2''-terpyridyl moiety, and a minor contribution is observed from the ferrocenyl moiety (Figure S32). On the other hand, the LUSO exhibits a majority of the probability density on the ferrocenyl moiety of the complex (67% contribution from Fe 3d orbitals), with minor contribution from the ruthenium(II) center and the bridging acetylide group. Therefore, the NIR electronic transition at 1127 nm, arising from the HOSO-26 to LUSO, can be described by a charge transfer from Ru(II) to Fe(III) in the singly oxidized species, 5^+ (Figure S32, Table S9).

CONCLUSIONS

In conclusion, we have designed, synthesized, and characterized a series of Ru(II)–Fe(II) heterobimetallic organometallic *wires* by varying the substituents on the terminal terpyridyl ligands to tune the electronic communication between the metal termini. Electrochemical studies revealed two well-separated redox waves due to both inherent redox asymmetry and metal–metal interactions for the Ru(II)–Fe(II) heterobinuclear *dyads*. The reversible redox waves in the range of 0.28–0.33 V ($E_{1/2}$) originated from the oxidation of the Fe(II)/Fe(III) (Fc/Fc⁺) couple, while the consecutive reversible redox waves observed at $E_{1/2}$ of 0.98–1.02 V were due to the Ru(II)/Ru(III) couple. The high K_c value (0.11 – 1.73×10^{12}) in the Ru^{II}Fe^{III} mixed-valence intermediates ascribes strong electronic communication present between the two metal termini. However, the substituents on *tpy* ligands do not play a significant role in electrochemical communication between the two redox termini. Most interestingly, the heterobimetallic complexes showed NIR absorption ($\lambda_{\text{MM'CT}} = 1401$ – 1417 nm) induced by MM'CT after treating with 1 equiv of oxidant, $[(\eta^5\text{-Cp})_2\text{Fe}]^+$, showing remarkable molar extinction coefficient (ϵ) in the order of 10^3 M⁻¹ cm⁻¹. Moreover, the electronic coupling constant (H_{ab}) was calculated for the structurally characterized heterobimetallic *dyads* (**6** and **7**), and it was found to be in the range of 444–492 cm⁻¹. From electrochemical and UV–vis–NIR spectral studies, it can be concluded that the mixed-valence species of the heterobimetallic *wires* belong to the Robin and Day “Class II” categories of mixed-valence complexes. Moreover, the DFT calculations (spin density distribution analysis) reveal that the “Ru–C≡C–Fc” moiety heavily participates in redox processes (electrochemical communication) in the mono-oxidized mixed-valence species and the metal to metal electron transfer occurs from the ruthenium(II) center to the ferrocenyl moiety. This work clearly reveals a promising platform for further development of ferrocenyl capped terpyridyl Ru(II) complexes

by varying the electronic nature of the terpyridyl unit to modulate the intermetallic electronic communication and consequent NIR absorption. Further investigation on the modulation of electronic communication is underway in our laboratory by varying the ancillary ligand, bridging spacer, and redox-active metal termini to access novel heterobimetallic *wires* for the application in molecular electronics.

EXPERIMENTAL SECTION

General Considerations. All moisture sensitive reactions and manipulations were performed under an inert atmosphere of prepurified Ar or N₂ by using standard dual-manifold Schlenk lines. The glassware was oven-dried (at 180 °C) and cooled under vacuum. Dry DCM, methanol and CCl₄ were obtained by distillation over CaH₂, whereas Na/benzophenone was used for drying tetrahydrofuran and toluene. Unless otherwise mentioned all the chemicals were of analytical grade, obtained from Aldrich, and used without further purification. Metal precursor (RuCl₃·xH₂O) was acquired from Arora Matthey Ltd. For column chromatography, neutral Alumina was purchased from SRL chemicals. Thin layer chromatography (TLC) analysis was used to determine the eluting systems for column chromatography purifications. Solvents were evaporated under reduced pressure using a rotary evaporator. Acetynyl ferrocene,¹⁷ $[(\eta^5\text{-Cp})_2\text{Fe}][\text{BF}_4]$ ¹⁸ and Ru(PPh₃)₃Cl₂¹⁹ were synthesized following the literature reported procedure.

¹H (600, 500, and 400 MHz), ¹³C{¹H} (150, 125, and 100 MHz) and ³¹P{¹H} (162 MHz) NMR spectra were recorded with a Bruker Lambda spectrometer using CDCl₃ unless otherwise mentioned. Spectra were internally referenced to residual solvent peaks ($\delta = 7.26$ ppm for proton and $\delta = 77.23$ for carbon (middle peak) in CDCl₃ or an external capillary of 85% H₃PO₄ for ³¹P{¹H} NMR. All coupling constants (J) are given in Hz. The HRMS mass spectra were recorded in ESI⁺ mode (70 eV) in Waters (Model: Xevo-G2QTOF) and Bruker MicrOTOF-Q-II mass spectrometers. Elemental analysis was carried out in a PerkinElmer Series II CHNS/O 2400 analyzer. The absorption spectra were collected using a Shimadzu (Model UV-2450) spectrophotometer. Vis–NIR absorption spectra were recorded in a CARY-5000 UV–vis–NIR spectrophotometer. FTIR studies were performed using Spectrum-BX (PerkinElmer). Cyclic voltammetric studies were performed on a BASi Epsilon electrochemical workstation in DCM with 0.1 M tetra-*n*-butylammoniumhexafluorophosphate (TBAPF₆) as the supporting electrolyte. The working electrode was a BASi Pt disc electrode, the reference electrode was Ag/AgCl, whereas the auxiliary electrode was a Pt wire. The Fc/Fc⁺ couple shows the oxidation wave at $E_{1/2} = +0.51(70)$ V versus Ag/AgCl reference electrode under the same experimental set up.

X-ray Data Collections and Refinement. Single-crystal X-ray diffraction study was carried out on a Bruker-APEX-II CCD X-ray diffractometer equipped with an Oxford Instruments low-temperature attachment. Data were collected at 100(2) K using graphite-monochromated Mo K α radiation ($\lambda_{\alpha} = 0.71073$ Å). The frames were indexed, integrated, and scaled using the SMART and SAINT software package.²⁰ The SADABS program was used for absorption correction.²¹ The single crystals were harvested on an 8 mm O.D. sealed glass tube. For complexes **3** and **7**, one independent molecule was located in the asymmetric unit. For complex **6**, two independent molecules were present in the asymmetric unit with negligible differences in their metrical parameters. These data can be obtained free of charge from The Cambridge Crystallographic Data Centre via www.ccdc.cam.ac.uk/data_request/cif. The structures were solved by SHELXT²² and refined with SHELXL²³ using the Olex2 program.²⁴ The molecular structure was generated by using ORTEP-3 for Windows Version 2.02.37.²⁵ Because of the failure to identify the disordered solvent molecules in complexes **6** and **7**, the SQUEEZE option in the PLATON program was used to remove the unidentified intensities from the overall intensity data.²⁶ The hydrogen atoms were included in geometrically calculated positions in the final stages of the refinement and were refined according to the typical riding model. All

non-hydrogen atoms were refined with anisotropic thermal parameters.

Computational Details. The geometries of complexes 5–8 were optimized using density functional theory with the hybrid CAM-B3LYP functional that takes care of long-range interactions.²⁷ The Fe and Ru metal centers were described by the LANL2DZ basis set,²⁸ while the 6-31G** basis set²⁹ was employed for all other atoms. Starting from the optimized geometries of the complexes in their nonoxidized states (where both the metal centers are in +2 oxidation state), the geometry was also optimized for the one-electron oxidized species of the complexes 5–8. The basis set and functional used for the nonoxidized complexes were also used for the one-electron oxidized species. All the optimized geometries were subjected to further confirmation by carrying out Hessian calculations. The electronic transitions from the ground electronic state to the excited states of all the complexes as well as their one-electron oxidized counterparts were evaluated by carrying out TDDFT calculations.³⁰ All calculations were carried out using the Gaussian 09 program.³¹ The orbital composition analysis of the resultant wave functions was performed using the Multiwfn program.³²

Synthesis and Characterization. Ligands L1–L4 have been synthesized following the literature procedure (SI).¹⁴

Synthesis of 4'-(Aryl)-2,2':6',2''-terpyridyl Ru(II) complexes.

Complex 1. In an oven-dried Schlenk flask, a mixture of 4'-(phenyl)-2,2':6',2''-terpyridine (0.031 g, 0.1 mmol) and RuCl₂(PPh₃)₃ (0.096 g, 0.1 mmol) and degassed MeOH (12 mL) were added and heated to reflux for 24 h under argon atmosphere. After cooling to room temperature, the reaction mixture was filtered through a bed of Celite, which was washed several times by dry MeOH (3 × 5 mL). Then NaPF₆ (0.265 g, 1.6 mmol) was charged to the concentrated solution, and it was left in the freezer for overnight to precipitate a brown fine crystalline solid product. After filtration, the solid was washed with diethyl ether (3 × 10 mL) and dried under vacuum to achieve analytically pure complex 1. Yield: 0.089 g, (80%). ¹H NMR (CDCl₃, 600 MHz): δ 7.08–7.19 (m, 14H), 7.20–7.23 (m, 17H), 7.53–7.56 (m, 2H), 7.58–7.66 (m, 4H), 7.72–7.75 (m, 4H, Py), 7.94 (d, J = 6 Hz, 2H, Py), 9.05 (d, J = 6 Hz, 2H, Py); ³¹P{¹H}NMR (CDCl₃, 162 MHz) δ 20.0 (s, PPh₃), –143.6 (septet, PF₆); ¹³C{¹H} NMR (CDCl₃, 150 MHz): δ 114.1, 120.5, 122.6, 126.2, 127.1, 128.2, 128.5, 129.7, 129.9, 131.9, 132.1, 132.9, 133.0, 136.2, 136.6, 139.6, 145.8, 155.3, 157.2, 158.0; FTIR (KBr, $\bar{\nu}$, cm⁻¹): 844 (PF₆); HRMS ESI⁺ (m/z): 970.1848 ([M-PF₆]⁺, calcd: 970.1821).

Complex 2. Treating 4'-(4-methylphenyl)-2,2':6',2''-terpyridine (0.032 g, 0.1 mmol) with RuCl₂(PPh₃)₃ (0.096 g, 0.1 mmol) in degassed MeOH (12 mL) under reflux condition, followed by addition of NaPF₆ (0.265 g, 1.6 mmol) yielded complex 2. Yield: 0.096 g, (86%). ¹H NMR (CDCl₃, 400 MHz): δ 2.49 (s, methyl 3H), 7.07–7.10 (m, PPh₃ 14H), 7.20–7.28 (m, 18H), 7.45 (d, J = 8 Hz, 2H), 7.65–7.67 (m, J = 8 Hz, 4H, Py), 7.73 (t, J = 8 Hz, 2H, Py), 7.94 (d, J = 8 Hz, 2H, Py), 9.05 (d, J = 4 Hz, 2H, Py); ³¹P{¹H} NMR (CDCl₃, 162 MHz): δ 20.2 (s, PPh₃), –143.6 (septet, PF₆); ¹³C{¹H} NMR (CDCl₃, 100 MHz): δ 21.4, 120.2, 122.6, 126.1, 126.9, 128.2, 128.5, 128.6, 129.7, 129.8, 129.9, 130.1, 130.5, 132.0, 132.1, 132.9, 133.3, 136.6, 140.5, 145.9, 155.3, 157.1, 158.1; FTIR (KBr, $\bar{\nu}$, cm⁻¹): 845 (PF₆); HRMS ESI⁺ (m/z): 984.1983 ([M-PF₆]⁺, calcd: 984.1977).

Complex 3. 3 was prepared using a similar procedure as described for complex 1, by treating RuCl₂(PPh₃)₃ (0.096 g, 0.1 mmol) and 4'-(4-fluorophenyl)-2,2':6',2''-terpyridine (0.033 g, 0.1 mmol) in degassed MeOH (12 mL) under refluxing condition followed by anion exchange using NaPF₆ (0.265 g, 1.6 mmol). Yield: 0.096 g, (87%). ¹H NMR (CDCl₃, 600 MHz): δ 7.05–7.08 (m, 14H), 7.17–7.21 (m, 20H), 7.62 (m, 2H), 7.70–7.76 (m, 4H, Py), 7.94 (d, J = 6 Hz, 2H, Py), 9.03 (d, J = 6 Hz, 2H, Py); ³¹P{¹H} NMR (CDCl₃, 162 MHz): δ 19.9 (s, PPh₃), –143.6 (septet, PF₆); ¹³C{¹H} NMR (CDCl₃, 150 MHz): δ 116.8, 116.9, 120.2, 122.7, 126.2, 128.2, 128.3, 129.1, 129.2, 129.7, 129.8, 129.9, 130.0, 132.9, 133.0, 136.6, 155.3, 157.3, 157.9; FTIR (KBr, $\bar{\nu}$, cm⁻¹): 840 (PF₆); HRMS ESI⁺ (m/z): 988.1804 ([M-PF₆]⁺, calcd: 988.1727).

Complex 4. 4 was prepared using a similar procedure for the synthesis of complex 1. RuCl₂(PPh₃)₃ (0.096 g, 0.1 mmol) and 4'-(4-dimethylaminophenyl)-2,2':6',2''-terpyridine (0.035 g, 0.1 mmol) were reacted in degassed MeOH (12 mL) under refluxing condition. Anion exchange by charging NaPF₆ (0.265 g, 1.6 mmol) produced cationic ruthenium(II) complex 4. Yield: 0.097 g, (84%). ¹H NMR (CDCl₃, 600 MHz): δ 9.02–9.01 (m, 2H, Py), 7.88–7.86 (m, 2H, Py), 7.71–7.64 (m, 4H, Py), 7.58 (s, 2H, Py), 7.20–7.17 (m, 18H), 7.07–7.03 (m, 14H), 6.90–6.88 (m, 2H), 3.10 (s, 6H, NMe₂); ³¹P{¹H} NMR (CDCl₃, 162 MHz) δ 20.0 (s PPh₃), –143.5 (septet, PF₆); ¹³C{¹H} NMR (125 MHz, CDCl₃) δ 158.6, 156.9, 155.5, 151.8, 146.4, 136.7, 133.2, 132.3, 130.5, 130.4, 129.9, 128.4, 128.2, 126.1, 123.1, 122.6, 119.2, 112.9, 40.5 (NMe₂); FTIR (KBr, $\bar{\nu}$, cm⁻¹): 842 (PF₆); HRMS ESI⁺ (m/z): 1013.2205 ([M-PF₆]⁺, calcd: 1013.2243).

Synthesis of Ru(II)–Fe(II) Heterobimetallic Wires. Complex 5.

In a 100 mL Schlenk flask, a solution of complex 1 (100 mg, 0.089 mmol), ethynylferrocene (38 mg, 0.18 mmol), and KF (15 mg, 0.22 mmol) in dry THF (5 mL) and CH₃OH (20 mL) was heated to reflux under Ar atmosphere for 24 h to form deep brown red solution. After cooling, the solvent was evaporated to a minimum volume (ca. 2 mL) and the crude product was precipitated after addition of dry diethyl ether (10 mL) through a syringe. The crude product was filtered through a Schlenk frit, and washed with hexanes. The product was purified by neutral alumina column chromatography (1.8 cm dia, 6 cm alumina packed bed) using distilled methanol as an eluent to collect the second band to afford an analytically pure brown solid of 5. Yield: 0.063 g (62%). ¹H NMR (CDCl₃, 600 MHz): δ (ppm) 8.82–8.79 (m, 2H, Py), 7.94–7.87 (m, 2H, Py), 7.75–7.72 (m, 4H, Py), 7.63–7.61 (m, 4H), 7.52–7.36 (m, 10 H), 7.22–7.18 (m, 6H), 7.10–7.07 (m, 15H), 6.89–6.87 (m, 2H), 4.48–4.15 (m, 9H, Fc). ¹³C{¹H} (CDCl₃, 125 MHz): δ 157.9, 156.6, 155.3, 146.8, 136.9, 136.3, 133.2, 131.9, 131.1, 130.9, 130.7, 130.2, 129.9, 129.8, 128.5, 128.4, 128.3, 127.5, 126.1, 122.8, 120.3, 70.1, 69.9, 69.7, 69.3; ³¹P{¹H} (CDCl₃, 162 MHz): 28.5 ppm (s, PPh₃), –143.9 (septet, PF₆); FTIR (KBr, $\bar{\nu}$, cm⁻¹): 840 (PF₆), 2070 (C≡C); HRMS ESI⁺ (m/z): 1144.2102 ([M-PF₆]⁺, calcd: 1144.2185); Anal. Calcd for C₆₉H₅₄N₃P₃F₆RuFe: C, 64.29; H, 4.22; N, 3.26. Found: C, 63.48; H, 4.05; N, 3.45.

Complex 6. 6 was prepared using a similar procedure as that for complex 5. A mixture of complex 2 (100 mg, 0.082 mmol), ethynylferrocene (37 mg, 0.176 mmol), and KF (15 mg, 0.22 mmol) in dry THF (5 mL) and CH₃OH (20 mL) was heated to reflux under Ar atmosphere for 24 h. The product was purified by neutral alumina column chromatography using distilled methanol as eluent to collect the second band to afford an analytically pure brown solid of 6. Yield: 0.056 g (60%). ¹H NMR (CDCl₃, 600 MHz): δ (ppm) 8.87–8.85 (m, 2H, Py), 7.94–7.87 (m, 2H, Py), 7.78–7.72 (m, 4H, Py), 7.65–7.61 (m, 2H, Py), 7.40–7.37 (m, 11 H), 7.21–7.18 (m, 6H), 7.10–7.08 (m, 15H), 6.91–6.87 (m, 2H), 4.25–4.17 (m, 9H, Fc), 2.16 (s, 3H, -Me). ¹³C{¹H} (CDCl₃, 150 MHz): δ 158.5, 156.5, 155.3, 147.2, 140.7, 136.3, 134.0, 133.2, 132.3, 131.2, 131.0, 130.9, 130.7, 129.8, 128.8, 128.2, 127.3, 126.1, 122.8, 120.1, 69.7, 69.6, 69.5, 69.4, 21.6 (methyl); ³¹P{¹H} (CDCl₃, 162 MHz): 28.1 ppm (s, PPh₃), –143.6 (septet, PF₆); FTIR (KBr, $\bar{\nu}$, cm⁻¹): 842 (PF₆); 2063 (C≡C); HRMS ESI⁺ (m/z): 1158.2356 ([M-PF₆]⁺, calcd: 1158.2343); Anal. Calcd for C₇₀H₅₆N₃P₃F₆RuFe: C, 64.52; H, 4.33; N, 3.22. Found: C, 64.03; H, 4.39; N, 3.37.

Complex 7. A solution of 3 (100 mg, 0.086 mmol), ethynylferrocene (37 mg, 0.172 mmol), and KF (13 mg, 0.21 mmol) in dry THF (5 mL) and CH₃OH (20 mL) was heated to reflux under Ar atmosphere for 24 h to form a deep brown red solution. Following the similar procedure as described for 6, the product was purified by neutral alumina column chromatography using distilled methanol as an eluent to afford complex 7. Yield: 0.066 g (66%). ¹H NMR (CDCl₃, 600 MHz): δ (ppm) 8.85–8.84 (m, 2H, Py), 7.93 (d, J = 6 Hz, 2H, Py), 7.80–7.78 (m, 2H, Py), 7.72 (s, 2H, Py), 7.64–7.61 (m, 2H, Py), 7.39–7.38 (m, 10H), 7.29–7.27 (m, 2H), 7.21–7.18 (m, 6H), 7.10–7.08 (m, 14H), 6.90–6.88 (m, 2H), 4.28–4.18 (m, 9H, Fc); ¹³C{¹H} (CDCl₃, 100 MHz): δ 157.9, 156.7, 155.3, 145.7, 136.4, 133.2, 133.1, 131.1, 130.9, 130.7, 129.7, 129.5, 129.4, 128.2, 126.1, 122.9, 120.1, 117.1, 116.9, 70.1, 69.6, 69.4, 67.4;

$^{31}\text{P}\{^1\text{H}\}$ (CDCl_3 , 162 MHz): 27.9 ppm (s, PPh_3), -143.5 (septet, PF_6); FTIR (KBr , $\bar{\nu}$, cm^{-1}): 835 (PF_6), 2069 ($\text{C}\equiv\text{C}$); HRMS ESI^+ (m/z): 1162.2069 ($[\text{M-PF}_6]^+$, calcd: 1162.2091); Anal. Calcd for $\text{C}_{69}\text{H}_{53}\text{N}_3\text{P}_3\text{F}_7\text{RuFe}$: C, 63.41; H, 4.09, N, 3.21. Found: C, 62.98, H, 3.92, N, 3.22.

Complex 8. Complex 8 was prepared and purified using an identical procedure as that for 5, by charging complex 4 (100 mg, 0.086 mmol), ethynylferrocene (36 mg, 0.172 mmol) and KF (13 mg, 0.21 mmol) in dry THF (5 mL) and CH_3OH (20 mL). Yield: 0.064 g (63%). ^1H NMR (CDCl_3 , 600 MHz): δ (ppm) 8.81–8.80 (m, 2H, Py), 8.24–8.23 (m, 2H), 7.98 (s, 2H), 7.88 (d, $J = 6$ Hz, 2H), 7.70 (d, $J = 6$ Hz, 2H), 7.38–7.37 (m, 11H), 7.20–7.17 (m, 6H), 7.09–7.06 (m, 13H), 6.93–6.84 (m, 4H), 4.24–4.13 (m, 9H, Fc), 3.11 (s, 6H, NMe_2); $^{13}\text{C}\{^1\text{H}\}$ (CDCl_3 , 100 MHz): δ 158.5, 156.7, 154.8, 136.4, 133.2, 131.4, 131.2, 131.0, 129.7, 128.5, 128.2, 125.8, 123.7, 123.2, 119.0, 118.5, 112.9, 69.6, 69.4, 69.3, 67.0, 40.5 (NMe_2). $^{31}\text{P}\{^1\text{H}\}$ (CDCl_3 , 162 MHz): 28.1 ppm (s, PPh_3), -143.6 (septet, PF_6); FTIR (KBr , $\bar{\nu}$, cm^{-1}): 844 (PF_6); 2070 ($\text{C}\equiv\text{C}$); HRMS ESI^+ (m/z): 1187.2685 ($[\text{M-PF}_6]^+$, calcd: 1187.2607); Anal. Calcd for $\text{C}_{71}\text{H}_{59}\text{N}_4\text{P}_3\text{F}_6\text{RuFe}$: C, 64.02; H, 4.46; N, 4.21. Found: C, 63.76; H, 4.47; N, 4.19.

■ ASSOCIATED CONTENT

Supporting Information

The Supporting Information is available free of charge on the ACS Publications website at DOI: 10.1021/acs.inorgchem.8b02440.

Experimental details; characterization data; photophysical, electrochemical, and theoretical studies; and crystallographic data (PDF)

Accession Codes

CCDC 1864202–1864204 contain the supplementary crystallographic data for this paper. These data can be obtained free of charge via www.ccdc.cam.ac.uk/data_request/cif, or by emailing data_request@ccdc.cam.ac.uk, or by contacting The Cambridge Crystallographic Data Centre, 12 Union Road, Cambridge CB2 1EZ, UK; fax: +44 1223 336033.

■ AUTHOR INFORMATION

Corresponding Authors

*E-mail: skpatra@chem.iitkgp.ac.in. Tel: +913222283338 (S.K.P.).

*E-mail: mishra@chem.iitkgp.ac.in. Tel: +913222282328 (S.M.).

ORCID

Sabyashachi Mishra: 0000-0002-2551-1021

Sanjib K. Patra: 0000-0002-1591-6762

Notes

The authors declare no competing financial interest.

■ ACKNOWLEDGMENTS

IIT Kharagpur is acknowledged for funding the purchase of an electrochemical workstation through a Competitive Research Infrastructure Seed Grant (IIT/SRIC/CHY/PBR/2014-15/44). The authors acknowledge DST (India) for funding a 500 MHz NMR spectrometer (SR/FST/CSII-026/2013). Central Research Facility, IIT Kharagpur, is gratefully acknowledged for the analytical facility. AS acknowledges IIT Kharagpur, and UG thanks CSIR, while VKM thanks UGC for doctoral fellowship.

■ REFERENCES

- (1) (a) Aguirre-Etcheverry, P.; O'Hare, D. Electronic communication through unsaturated hydrocarbon bridges in homobimetallic organometallic complexes. *Chem. Rev.* **2010**, *110*, 4839–4864. (b) Olivier, C.; Costuas, K.; Choua, S.; Maurel, V.; Turek, P.; Saillard, J. – Y.; Touchard, D.; Rigaut, S. Chain-like” trimetallic ruthenium complexes with C7 carbon-rich bridges: experimental and theoretical investigations of electronic communication tuning in five distinct oxidation states. *J. Am. Chem. Soc.* **2010**, *132*, 5638–5651. (c) Chisholm, M. H.; Lear, B. J. $\text{M}2\delta$ to ligand π -conjugation: testbeds for current theories of mixed valence in ground and photoexcited states of molecular systems. *Chem. Soc. Rev.* **2011**, *40*, 5254–5265. (d) Yoshida, J.; Kuwahara, K.; Suzuki, K.; Yuge, H. Long-range intramolecular electronic communication in a trinuclear ruthenium tropolonate complex. *Inorg. Chem.* **2017**, *56*, 1846–1856.
- (2) (a) Kaim, W. Concepts for metal complex chromophores absorbing in the near infrared. *Coord. Chem. Rev.* **2011**, *255*, 2503–2513. (b) Cui, B. B.; Yao, C.-J.; Yao, J.; Zhong, Y. W. Electropolymerized films as a molecular platform for volatile memory devices with two near-infrared outputs and long retention time. *Chem. Sci.* **2014**, *5*, 932–941. (c) Milan, D. C.; Vezzoli, A.; Planje, I. J.; Low, P. J. Metal bis(acetylide) complex molecular wires: concepts and design strategies. *Dalton Trans* **2018**, *47*, 14125–14138. (d) Tanaka, Y.; Kiguchi, M.; Akita, M. Inorganic and organometallic molecular wires for single-molecule devices. *Chem. - Eur. J.* **2017**, *23*, 4741–4749. (e) Tanaka, Y.; Kato, Y.; Tada, T.; Fujii, S.; Kiguchi, M.; Akita, M. Doping of polyyne with an organometallic fragment leads to highly conductive metallapolyne molecular wire. *J. Am. Chem. Soc.* **2018**, *140*, 10080–10084. (f) Haque, A.; Al-Balushi, R. A.; Al-Busaidi, I. J.; Khan, M. S.; Raithby, P. R. Rise of conjugated poly-ynes and poly(metalla-ynes): from design through synthesis to structure-property relationships and applications. *Chem. Rev.* **2018**, *118*, 8474–8597.
- (3) (a) Simao, C.; Mas-Torrent, M.; Crivillers, N.; Lloveras, V.; Artes, J. M.; Gorostiza, P.; Veciana, J.; Rovira, C. A robust molecular platform for non-volatile memory devices with optical and magnetic responses. *Nat. Chem.* **2011**, *3*, 359–364. (b) Terada, K.; Kanaizuka, K.; Iyer, V. M.; Sannodo, M.; Saito, S.; Kobayashi, K.; Haga, M. Memory effects in molecular films of free-standing rod-shaped ruthenium complexes on an electrode. *Angew. Chem., Int. Ed.* **2011**, *50*, 6287–6291. (c) Gong, Z. L.; Yao, C. J.; Shao, J. Y.; Nie, H. J.; Tang, J. H.; Zhong, Y. W. Redox-responsive carbometalated ruthenium and osmium complexes. *Sci. China: Chem.* **2017**, *60*, 583–590.
- (4) (a) He, X.; Yam, V. W. -W. Luminescent gold(I) complexes for chemosensing. *Coord. Chem. Rev.* **2011**, *255*, 2111–2123. (b) Zhao, Q.; Li, F.; Huang, C. Phosphorescent chemosensors based on heavy-metal complexes. *Chem. Soc. Rev.* **2010**, *39*, 3007–3030. (c) Guerchais, V.; Fillaut, J.-L. Sensory luminescent iridium(III) and platinum(II) complexes for cation recognition. *Coord. Chem. Rev.* **2011**, *255*, 2448–2457. (d) Ma, D. L.; Ma, V. P. Y.; Chan, D. S. H.; Leung, K. H.; He, H. Z.; Leung, C. H. Recent advances in luminescent heavy metal complexes for sensing. *Coord. Chem. Rev.* **2012**, *256*, 3087–3113.
- (5) (a) Bechlars, B.; D'Alessandro, D. M.; Jenkins, D. M.; Iavarone, A. T.; Glover, S. D.; Kubiak, C. P.; Long, J. R. High-spin ground states via electron delocalization in mixed-valence imidazolate-bridged divanadium complexes. *Nat. Chem.* **2010**, *2*, 362–368. (b) Šalitroš, I.; Boča, R.; Herchel, R.; Moncol, J.; Nemeč, I.; Ruben, M.; Renz, F. Mixed-valence heptanuclear iron complexes with ferromagnetic interaction. *Inorg. Chem.* **2012**, *51*, 12755–12767.
- (6) (a) Mei, J.; Ogawa, K.; Kim, Y. G.; Heston, N. C.; Arenas, D. J.; Nasrollahi, Z.; McCarley, T. D.; Tanner, D. B.; Reynolds, J. R.; Schanze, K. S. Low-band-gap platinum acetylide polymers as active materials for organic solar cells. *ACS Appl. Mater. Interfaces* **2009**, *1*, 150–161. (b) Zhao, X.; Piliago, C.; Kim, B.; Poulsen, D. A.; Ma, B.; Unruh, D. A.; Frechet, J. M. J. Solution-processable crystalline platinum-acetylide oligomers with broadband absorption for photovoltaic cells. *Chem. Mater.* **2010**, *22*, 2325–2332. (c) Wong, W. Y.;

- Wang, X. Z.; He, Z.; Chan, K. K.; Djurisić, A. B.; Cheung, K. Y.; Yip, C. T.; Ng, A. M. C.; Xi, Y. Y.; Mak, C. S. K.; Chan, W. K. Tuning the absorption, charge transport properties, and solar cell efficiency with the number of thiophene rings in platinum-containing poly(aryleneethynylene)s. *J. Am. Chem. Soc.* **2007**, *129*, 14372–14380.
- (d) Dai, F. R.; Zhan, H. M.; Liu, Q.; Fu, Y. Y.; Li, J. H.; Wang, Q. W.; Xie, Z.; Wang, L.; Yan, F.; Wong, W. Y. Platinum(II)–bis(aryleneethynylene) complexes for solution-processible molecular bulk heterojunction solar cells. *Chem. - Eur. J.* **2012**, *18*, 1502–1511.
- (e) Colombo, A.; Dragonetti, C.; Roberto, D.; Ugo, R.; Falciola, L.; Luzzati, S.; Kotowski, D. Novel diruthenium acetylide donor complex as an unusual active material for bulk heterojunction solar cells. *Organometallics* **2011**, *30*, 1279–1282.
- (7) (a) Launay, J. P. Electron transfer in molecular binuclear complexes and relation with electron transport through nanojunctions. *Coord. Chem. Rev.* **2013**, *257*, 1544–1554. (b) Sakamoto, R.; Katagiri, S.; Maeda, H.; Nishihara, H. Bis(terpyridine) metal complex wires: excellent long-range electron transfer ability and controllable intrawire redox conduction on silicon electrode. *Coord. Chem. Rev.* **2013**, *257*, 1493–1506. (c) Robertson, N.; McGowan, C. A. A comparison of potential molecular wires as components for molecular electronics. *Chem. Soc. Rev.* **2003**, *32*, 96–103.
- (8) (a) Creutz, C.; Taube, H. A direct approach to measuring the Franck-Condon barrier to electron transfer between metal ions. *J. Am. Chem. Soc.* **1969**, *91*, 3988–3989. (b) Creutz, C.; Taube, H. Binuclear complexes of ruthenium amines. *J. Am. Chem. Soc.* **1973**, *95*, 1086–1094.
- (9) (a) Ren, T. Diruthenium σ -alkynyl compounds: a new class of conjugated organometallics. *Organometallics* **2005**, *24*, 4854–4870. (b) Maurer, J.; Linseis, M.; Sarkar, B.; Schwederski, B.; Niemeyer, M.; Kaim, W.; Zališ, S.; Anson, C.; Zabel, M.; Winter, R. F. Ruthenium complexes with vinyl, styryl, and vinylpyrenyl ligands: a case of non-innocence in organometallic chemistry. *J. Am. Chem. Soc.* **2008**, *130*, 259–268. (c) Costuas, K.; Rigaut, S. Polynuclear carbon-rich organometallic complexes: clarification of the role of the bridging ligand in the redox properties. *Dalton Trans* **2011**, *40*, 5643–5658. (d) Wang, L.; Yang, W. W.; Zheng, R. H.; Shi, Q.; Zhong, Y. W.; Yao, J. Electronic coupling between two cyclometalated ruthenium centers bridged by 1,3,6,8-tetrakis(1-butyl-1H-1,2,3-triazol-4-yl)pyrene. *Inorg. Chem.* **2011**, *50*, 7074–7079. (e) Yao, C.-J.; Zhong, Y.-W.; Yao, J. Modulation of electronic couplings within Ru₂polyyne frameworks. *J. Am. Chem. Soc.* **2011**, *133*, 15697–15706. (f) Glover, S. D.; Kubiak, C. P. Persistence of the three-state description of mixed valency at the localized-to-delocalized transition. *J. Am. Chem. Soc.* **2011**, *133*, 8721–8731. (g) Kobayashi, K.; Ishikubo, M.; Kanaizuka, K.; Kosuge, K.; Masaoka, S.; Sakai, K.; Nozaki, K.; Haga, M. A. Electronic coupling and electron transfer between two dimolybdenum units spaced by a biphenylene group. *Chem. - Eur. J.* **2011**, *17*, 6954–6963. (h) Low, P. J. Twists and turns: studies of the complexes and properties of bimetallic complexes featuring phenylene ethynylene and related bridging ligands. *Coord. Chem. Rev.* **2013**, *257*, 1507–1532. (i) Halet, J.-F.; Lapinte, C. Charge delocalization vs localization in carbon-rich iron mixed-valence complexes: a subtle interplay between the carbon spacer and the (dppe)Cp*Fe organometallic electrophore. *Coord. Chem. Rev.* **2013**, *257*, 1584–1613. (j) Zhang, D. B.; Wang, J. Y.; Wen, H. M.; Chen, Z. N. Electrochemical, spectroscopic, and theoretical studies on diethynyl ligand bridged ruthenium complexes with 1,3-bis(2-pyridylimino)isoindolate. *Organometallics* **2014**, *33*, 4738–4746. (k) Xiao, X.; Meng, M.; Lei, H.; Liu, C. Y. Bridge-localized HOMO-binding character of divinylanthracene-bridged dinuclear ruthenium carbonyl complexes: spectroscopic, spectroelectrochemical, and computational studies. *J. Phys. Chem. C* **2014**, *118*, 8308–8315. (l) Ou, Y. P.; Zhang, J.; Xu, M.; Xia, J.; Hartl, F.; Yin, J.; Yu, G.; Liu, S. H. Bridge-localized homo-binding character of divinylanthracene-bridged dinuclear ruthenium carbonyl complexes: spectroscopic, spectroelectrochemical, and computational studies. *Chem. - Asian J.* **2014**, *9*, 1152–1160. (m) Das, H. S.; Schweinfurth, D.; Fiedler, J.; Khusniyarov, M. M.; Mobin, S. M.; Sarkar, B. Tuning the electronic properties in ruthenium–quinone complexes through metal coordination and substitution at the bridge. *Chem. - Eur. J.* **2014**, *20*, 4334–4346. (n) Yao, C. J.; Nie, H. J.; Yang, W. W.; Yao, J.; Zhong, Y. W. Combined experimental and computational study of pyren-2,7-diyl-bridged diruthenium complexes with various terminal ligands. *Inorg. Chem.* **2015**, *54*, 4688–4698. (o) Pfaff, U.; Hildebrandt, A.; Korb, M.; Oswald, S.; Linseis, M.; Schreiter, K.; Spange, S.; Winter, R. F.; Lang, H. Electronically strongly coupled divinylheterocyclic-bridged diruthenium complexes. *Chem. - Eur. J.* **2016**, *22*, 783–801. (p) Zhong, Y. W.; Gong, Z. L.; Shao, J. Y.; Yao, J. Electronic coupling in cyclometalated ruthenium complexes. *Coord. Chem. Rev.* **2016**, *312*, 22–40. (q) Mandal, A.; Hoque, M. A.; Grupp, A.; Paretzki, A.; Kaim, W.; Lahiri, G. K. Analysis of redox series of unsymmetrical 1,4-diamido-9,10-anthraquinone-bridged diruthenium compounds. *Inorg. Chem.* **2016**, *55*, 2146–2156. (r) Zhang, J.; Guo, S. J.; Dong, Y. B.; Rao, L.; Yin, J.; Yu, G. A.; Hartl, F.; Liu, S. H. Multistep oxidation of diethynyl oligophenylamine-bridged diruthenium and diiron complexes. *Inorg. Chem.* **2017**, *56*, 1001–1015. (s) Mackenzie, C. F. R.; Bock, S. R.; Lim, C. Y.; Skelton, B. W.; Nervi, C.; Wild, D. A.; Low, P. J.; Koutsantonis, G. A. Coordinating tectons. Experimental and computational infrared data as tools to identify conformational isomers and explore electronic structures of 4-ethynyl-2,2'-bipyridine complexes. *Organometallics* **2017**, *36*, 1946–1961. (t) Ou, Y. – P.; Zhang, J.; Zhang, M. – X.; Zhang, F.; Kuang, D.; Hartl, F.; Liu, S. H. *Inorg. Chem.* **2017**, *56*, 11074–11086. (u) Saha Roy, S.; Sil, A.; Giri, D.; Chowdhury, S. R.; Mishra, S.; Patra, S. K. Diruthenium(II)-capped oligothiophenyl ethynyl bridged highly soluble organometallic wires exhibiting long-range electronic coupling. *Dalton Trans* **2018**, *47*, 14304.
- (10) (a) Paul, F.; Lapinte, C. Organometallic molecular wires and other nanoscale-sized devices. An approach using the organoiron (dppe)Cp*Fe building block. *Coord. Chem. Rev.* **1998**, *178*, 431–509. (b) Kaim, W.; Sarkar, B. Mixed valency in ruthenium complexes coordinative aspects. *Coord. Chem. Rev.* **2007**, *251*, 584–594. (c) Zališ, S.; Winter, R. F.; Kaim, W. Quantum chemical interpretation of redox properties of ruthenium complexes with vinyl and TCNX type non-innocent ligands. *Coord. Chem. Rev.* **2010**, *254*, 1383–1396.
- (11) (a) Sato, M.; Shintate, H.; Kawata, Y.; Sekino, M. Oxidized ruthenium ferrocenylacetylide complexes, $[(\eta\text{-C}_5\text{H}_5)_2\text{RuCCFc}] \text{PF}_6$ and $[(\eta\text{-C}_5\text{Me}_5)_2\text{RuCCFc}] \text{PF}_6$ (L = Phosphines) electron-delocalized heterobinuclear mixed-valence complexes. *Organometallics* **1994**, *13*, 1956–1962. (b) Colbert, M. C. B.; Ingham, S. L.; Lewis, J.; Long, N. J.; Raithby, P. R. Synthetic and structural characterisation of metal complexes of ferrocenylacetylene: novel donor-acceptor heterobimetallic materials. *J. Chem. Soc., Dalton Trans.* **1994**, 2215–2216. (c) Sato, M.; Hayashi, Y. Synthesis and oxidation of iron(II) ferrocenylacetylide diphosphine complexes. A novel type of mixed-valence complex. *Organometallics* **1996**, *15*, 721–728. (d) Colbert, M. C. B.; Lewis, J.; Long, N. J.; Raithby, P. R.; White, A. J. P.; Williams, D. J. Synthetic, structural, electrochemical and electronic characterisation of heterobimetallic bis(acetylide) ferrocene complexes. *J. Chem. Soc., Dalton Trans.* **1997**, 99–104. (e) Paul, F.; Meyer, W. E.; Toupet, L.; Jiao, H.; Gladysz, J. A.; Lapinte, C. A. Conjugal[†] consanguineous family of butadiynediyl-derived complexes: synthesis and electronic ground states of neutral, radical cationic, and dicationic iron/ruthenium C4 species. *J. Am. Chem. Soc.* **2000**, *122*, 9405–9414. (f) Yuan, P.; Liu, S. H.; Xiong, W.; Yin, J.; Yu, G.; Sung, H. Y.; Williams, I. D.; Jia, G. Synthesis and characterization of (CH₃CH)₃-bridged heterobimetallic ferrocene-ruthenium complexes. *Organometallics* **2005**, *24*, 1452–1457. (g) Bruce, M. I.; Low, P. J.; Hartl, F.; Humphrey, P. A.; Montigny, F.; Jevric, M.; Lapinte, C.; Perkins, G. J.; Roberts, R. L.; Skelton, B. W.; White, A. H. Syntheses, structures, some reactions, and electrochemical oxidation of ferrocenylethynyl complexes of iron, ruthenium, and osmium. *Organometallics* **2005**, *24*, 5241–5255. (h) Smith, M. E.; Flynn, E. L.; Fox, M. A.; Trotter, A.; Wrede, E.; Yufit, D. S.; Howard, J. A. K.; Ronayne, K. L.; Towrie, M.; Parker, A. W.; Hartl, F.; Low, P. J. Facile photoinduced charge separation through a cyanoacetylide bridge in a heterobimetallic

- Fe(II)–Re(I) complex. *Chem. Commun.* **2008**, 5845–5847. (i) Lin, Y.-C.; Chen, W.-T.; Tai, J.; Su, D.; Huang, S.-Y.; Lin, I.; Lin, J.-L.; Lee, M. M.; Chiou, M. F.; Liu, Y.-H.; Kwan, K.-S.; Chen, Y.-J.; Chen, H.-Y. Tuning through-bond Fe(III)/Fe(II) coupling by solvent manipulation of a central ruthenium redox couple. *Inorg. Chem.* **2009**, *48*, 1857–1870. (j) Kowalski, K.; Linseis, M.; Winter, R. F.; Zabel, M.; Zális, S.; Kelm, H.; Kruger, H.-J.; Sarkar, B.; Kaim, W. Charge delocalization in a heterobimetallic ferrocene-(vinyl)Ru(CO)-Cl-(PⁱPr₃)₂ System. *Organometallics* **2009**, *28*, 4196–4209. (k) Wu, K.-Q.; Guo, J.; Yan, J.-F.; Xie, L.-L.; Xu, F.-B.; Bai, S.; Nockemann, P.; Yuan, Y.-F. Ruthenium(II) bis(terpyridine) electron transfer complexes with alkynyl–ferrocenyl bridges: synthesis, structures, and electrochemical and spectroscopic studies. *Dalton Trans* **2012**, *41*, 11000–11008. (l) Lohan, M.; Justaud, F.; Lang, H.; Lapinte, C. Synthesis, spectroelectrochemical, and EPR spectroscopic studies of mixed bis(alkynyl)biferrocenes of the type (LnMC≡C)(LnM'C≡C)-bfc. *Organometallics* **2012**, *31*, 3565–3574. (m) Wu, S. H.; Shen, J. J.; Yao, J.; Zhong, Y. W. Asymmetric mixed-valence complexes that consist of cyclometalated ruthenium and ferrocene: synthesis, characterization, and electronic-coupling studies. *Chem. - Asian J.* **2013**, *8*, 138–147. (n) Wen, H. M.; Wang, J. Y.; Zhang, L. Y.; Shi, L. X.; Chen, Z. N. Syntheses, characterization and electrochemical and spectroscopic properties of ruthenium–iron complexes of 2,3,5,6-tetrakis(2-pyridyl)pyrazine and ferrocene-acetylide ligands. *Dalton Trans* **2016**, *45*, 10620–10629. (o) Wong, K. M.-C.; Lam, S. C.-F.; Ko, C.-C.; Zhu, N.; Yam, V. W.-W.; Roué, S.; Lapinte, C.; Fathallah, S.; Costuas, K.; Kahlal, S.; Halet, J.-F. Electroswitchable photoluminescence activity: synthesis, spectroscopy, electrochemistry, photophysics, and X-ray crystal and electronic structures of [Re-(bpy)(CO)₃(C≡C-C₆H₄-C≡C)Fe(C₅Me₅)(dppe)]_n[PF₆]_n (n = 0, 1). *Inorg. Chem.* **2003**, *42*, 7086–7097. (p) Bruce, M. L.; Costuas, K.; Davin, T.; Ellis, B. G.; Halet, J.-F.; Lapinte, C.; Low, P. J.; Smith, M. E.; Skelton, B. W.; Toupet, L.; White, A. H. Iron versus ruthenium: dramatic changes in electronic structure result from replacement of one Fe by Ru in [{Cp*(dppe)Fe}-CC-CC-{Fe(dppe)Cp*}]²⁺ (n = 0, 1, 2). *Organometallics* **2005**, *24*, 3864–3881. (q) Gauthier, N.; Olivier, C.; Rigaut, S.; Touchard, D.; Roisnel, T.; Humphrey, M. G.; Paul, F. Intramolecular optical electron transfer in mixed-valent dinuclear iron–ruthenium complexes featuring a 1,4-diethynylaryl spacer. *Organometallics* **2008**, *27*, 1063–1072. (r) Fitzgerald, E. C.; Ladjarafi, A.; Brown, N. J.; Collison, D.; Costuas, K.; Edge, R.; Halet, J.-F.; Low, P. J.; Meghezzi, H.; Roisnel, T.; Whitely, M. W.; Lapinte, C. Spectroscopic evidence for redox isomerism in the 1,4-diethynylbenzene-bridged heterobimetallic cation [{Fe(dppe)Cp*}-(μ -C≡C-C₆H₄-C≡C){Mo(dppe)(η -C₇H₇)}]PF₆. *Organometallics* **2011**, *30*, 4180–4195. (s) Wu, S. H.; Shao, J. Y.; Kang, H. W.; Yao, J.; Zhong, Y. W. Substituent and solvent effects on the electrochemical properties and intervalence transfer in asymmetric mixed-valent complexes consisting of cyclometalated ruthenium and ferrocene. *Chem. - Asian J.* **2013**, *8*, 2843–2850.
- (12) Robin, M. B.; Day, P. Mixed valence chemistry—a survey and classification. *Adv. Inorg. Chem. Radiochem.* **1968**, *10*, 247–422.
- (13) (a) Allen, G.; Hush, N. Intervalence-transfer absorption. Part I. Qualitative evidence for intervalence-transfer absorption in inorganic systems in solution and in the solid state. *Prog. Inorg. Chem.* **2007**, *8*, 357–389. (b) Hush, N. S. Intervalence–transfer absorption. II. Theoretical considerations and spectroscopic data. *Prog. Inorg. Chem.* **2007**, *8*, 391–444. (c) Cecon, A.; Santi, S.; Orian, L.; Bisello, A. Electronic communication in heterobinuclear organometallic complexes through unsaturated hydrocarbon bridges. *Coord. Chem. Rev.* **2004**, *248*, 683–724.
- (14) Kröhnke, F. The specific synthesis of pyridines and oligopyridines. *Synthesis* **1976**, *1*, 1–24.
- (15) (a) Santi, S.; Bisello, A.; Cardena, R.; Donoli, A. Key multi(ferrocenyl) complexes in the interplay between electronic coupling and electrostatic interaction. *Dalton Trans* **2015**, *44*, 5234–5257. (b) Brunschwig, B. S.; Sutin, N. Energy surfaces, reorganization energies, and coupling elements in electron transfer. *Coord. Chem. Rev.* **1999**, *187*, 233–254. (c) Winter, R. F. Half-wave potential splittings $\Delta E_{1/2}$ as a measure of electronic coupling in mixed-valent systems: triumphs and defeats. *Organometallics* **2014**, *33*, 4517–4536.
- (16) Ghosh, B. N.; Topić, F.; Sahoo, P. K.; Mal, P.; Linnera, J.; Kalenius, E.; Tuononen, H. M.; Rissanen, K. Synthesis, structure and photophysical properties of a highly luminescent terpyridinediphenylacetylene hybrid fluorophore and its metal complexes. *Dalton Trans* **2015**, *44*, 254–267.
- (17) Rosenblum, M.; Brawn, N.; Papenmeier, J.; Applebaum, M. Synthesis of ferrocenylacetylenes. *J. Organomet. Chem.* **1966**, *6*, 173–180.
- (18) Connelly, N. G.; Geiger, W. E. Chemical Redox Agents for Organometallic Chemistry. *Chem. Rev.* **1996**, *96*, 877–910.
- (19) Hallman, P. S.; Stephenson, T. A.; Wilkinson, G. Tetrakis(triphenylphosphine)dichloro-ruthenium(II) and tris(triphenylphosphine)dichlororuthenium(II). *Inorganic Syntheses* **2007**, *12*, 237–240.
- (20) SAINT+ Software for CCD Diffractometers; Bruker AXS: Madison, WI, 2000.
- (21) Sheldrick, G. M. SADABS Program for Correction of Area Detector Data; University of Göttingen: Göttingen, Germany, 1999.
- (22) Sheldrick, G. M. SHELXT - Integrated Space-group and Crystal-structure Determination. *Acta Crystallogr., Sect. A: Found. Adv.* **2015**, *71*, 3–8.
- (23) Sheldrick, G. M. Crystal Structure Refinement with SHELXL. *Acta Crystallogr., Sect. C: Struct. Chem.* **2015**, *71*, 3–8.
- (24) Dolomanov, O. V.; Bourhis, L. J.; Gildea, R. J.; Howard, J. A. K.; Puschmann, H. OLEX2: A Complete Structure Solution, Refinement and Analysis Program. *J. Appl. Crystallogr.* **2009**, *42*, 339–341.
- (25) Farrugia, L. J. ORTEP-3 for windows - A Version of ORTEP-III with a Graphical User Interface (GUI). *J. Appl. Crystallogr.* **1997**, *30*, 565.
- (26) van der Sluis, P.; Spek, A. L. BYPASS: An Effective Method for the Refinement of Crystal Structures Containing Disordered Solvent Regions. *Acta Crystallogr., Sect. A: Found. Crystallogr.* **1990**, *46*, 194–201.
- (27) Yanai, T.; Tew, D. P.; Handy, N. C. A new hybrid exchange-correlation functional using the Coulomb-attenuating method (CAM-B3LYP). *Chem. Phys. Lett.* **2004**, *393*, 51–57.
- (28) (a) Hay, P. J.; Wadt, W. R. Ab initio effective core potentials for molecular calculations. potentials for the transition metal atoms Sc to Hg. *J. Chem. Phys.* **1985**, *82*, 270–283. (b) Hay, P. J.; Wadt, W. R. Ab initio effective core potentials for molecular calculations. Potentials for main group elements Na to Bi. *J. Chem. Phys.* **1985**, *82*, 284–298. (c) Hay, P. J.; Wadt, W. R. Ab initio effective core potentials for molecular calculations. Potentials for K to Au including the outermost core orbitals. *J. Chem. Phys.* **1985**, *82*, 299–310.
- (29) Hariharan, P. C.; Pople, J. A. Influence of polarization functions on molecular-orbital hydrogenation energies. *Theor. Chem. Acc.* **1973**, *28*, 213–225.
- (30) (a) Runge, E.; Gross, E. K. U. Density-Functional Theory for Time-Dependent Systems. *Phys. Rev. Lett.* **1984**, *52*, 997–1000. (b) Stratmann, R. E.; Scuseria, G. E. An efficient implementation of time-dependent density-functional theory for the calculation of excitation energies of large molecules. *J. Chem. Phys.* **1998**, *109*, 8218–8224. (c) Bauernschmitt, R.; Ahlrichs, R. Treatment of electronic excitations within the adiabatic approximation of time dependent density functional theory. *Chem. Phys. Lett.* **1996**, *256*, 454–264.
- (31) Frisch, M. J.; et al. *Gaussian 09*; Gaussian Inc.: Wallingford, CT, 2009.
- (32) Lu, T.; Chen, F. W. Multiwfn: A multifunctional wave function analyzer. *J. Comput. Chem.* **2012**, *33*, 580–592.